14th International Symposium on Turbulence and Shear Flow Phenomena (TSFP14)
Heidelberg, Germany, July 28–31, 2026

OBLIQUE MODES & SPATIOTEMPORAL LINEAR STABILITY OF PLANE COUETTE FLOW

K. Wilhelm[1,2], **N. Chandra**[1], **J. Conrad**[1,2], **S. Görtz**[1,2], **Y. Wang**[1], **M. Oberlack**[1,2]
[1]Chair of Fluid Dynamics, Technical University of Darmstadt, 64287 Darmstadt, Germany
[2]Center for Computational Engineering, Technical University of Darmstadt, 64293 Darmstadt, Germany
wilhelm@fdy.tu-darmstadt.de

ABSTRACT

Briggs' method determines the asymptotic behavior of linear initial-boundary value problems from the analytic structure of the dispersion relation in the complex wave number and frequency planes. A key challenge is the identification of admissible pinch points, which requires continuous deformation of the integration contours while preserving their topological relation to the eigenvalue spectrum.

In this work, a novel numerical approach is proposed in which the integration contours are treated as evolving curves in the complex planes. The contour deformation is formulated as a geometric gradient-flow problem driven by repulsive interactions with eigenvalue trajectories. The resulting evolution equations continuously deform the integration contours toward pinch points, which determine the asymptotic approximation of the linear initial-boundary value problem in Briggs' method. The method is validated using an analytic test dispersion relation with a known analytic pinch point and is intended for future application to spatiotemporal stability analyses of plane Couette flow.

INTRODUCTION

A classical theoretical guideline in linear stability theory is Squire's theorem. By comparing temporal normal modes in 2D and 3D, Squire (1933) demonstrated that each 2D modes is associated with a lower Reynolds number than its corresponding 3D counterpart. Consequently, the onset of instability through temporal normal modes is determined by 2D disturbances.

However, Squire's theorem applies only to temporal normal modes. Oberlack *et al.* (2026) extended the comparison between 2D and 3D disturbances to spatiotemporal normal modes. Interestingly, in this setting the conclusion of Squire's theorem may be reversed. Certain 3D perturbations may become unstable at Reynolds number below those of the associated 2D perturbation. i.e. subcritically. These 3D perturbations are called oblique modes, as they occur at an angle in the streamwise-spanwise plane.

However, the stability investigation of individual spatiotemporal normal modes is meaningless, since the spatial part of their eigenfunction grows without bound, even at the initial instant. Despite this, such modes remain useful within a framework like Briggs' method, where they appear only through a superposition of spatiotemporal modes.

Briggs' method, originally introduced by Briggs (1964) in the context of plasma physics, provides a framework for determining the asymptotic behavior of the linear initial-boundary value problem. The method relies on the analytic properties of the dispersion relation in the complex planes of wave frequency and wave number. Instead of considering individual spatiotemporal normal modes, it examines the interaction of singularities of the dispersion relation under analytic continuation and contour deformation. This analysis leads to the identification of pinch points and saddle points that control the asymptotic behavior to a perturbation. In this sense, Briggs' method assigns physical meaning to spatiotemporal modes through their collective contribution to the asymptotic behavior of the flow, physically corresponding to wave packets.

Wilhelm *et al.* (2026) applied the extended Squire transformation by Oberlack *et al.* (2026) to the physical initial-boundary value problem and showed that the asymptotic approximation of the 3D problem can be expressed in terms of a family of equivalent 2D problems within the framework of Briggs' method.

A variety of approaches have been proposed to numerically determine the location of such pinch points or saddle points. A naive approach would be to map out the dispersion relation $\mathcal{D}(\alpha, \omega)$ entirely.

For plane Poiseuille flow, Deissler (1987) assumed that a saddle point is initially located near the real wave number axis at the position corresponding to maximal temporal growth, and then followed its trajectory over a range of Reynolds numbers and varying observer velocities. The continuation was not extended all the way to pinch points, i.e. to vanishing observer velocity, because the lower neutral-growth rays remained associated with positive observer velocities and therefore represented convective instabilities. Together with an asymptotic analysis in the limit of large Reynolds numbers, this led him to conclude that instabilities in plane Poiseuille flow are exclusively convective.

Using Newton iterations with numerically approximated Jacobians, Sengupta & Orkwis (1996) computed pinch points directly in the complex wave number plane. Exploiting the analyticity of the dispersion relation, they formulated an efficient algorithm requiring only three eigenvalue evaluations per Newton step.

A limitation of these approaches is that the detection of a pinch point alone does not ensure that the spatial integration contour can be continuously deformed through it, like it is required in Briggs' method. In addition, it is generally unknown beforehand whether the branches responsible for the pinching originate from opposite half-planes, a requirement established by Bers (1983). When both branches emerge from the same half-plane, the integration contour may always be deformed continuously so as to avoid the singularity.

GOVERNING EQUATIONS

We analyze an incompressible Newtonian fluid governed by the nondimensional Navier-Stokes equations

$$\boldsymbol{\nabla} \cdot \boldsymbol{u} = 0, \tag{1a}$$

$$\frac{\partial \boldsymbol{u}}{\partial t} + (\boldsymbol{u} \cdot \boldsymbol{\nabla})\boldsymbol{u} = -\boldsymbol{\nabla} p + \frac{1}{Re}\nabla^2 \boldsymbol{u}, \text{ with } Re := \frac{\rho U_0 L}{\mu}, \tag{1b}$$

where $\boldsymbol{u}$, p, and Re denote velocity, pressure, and the Reynolds number, the latter comprising the density ρ, a characteristic velocity scale U_0, a characteristic length scale L, and the dynamic viscosity μ.

We introduce a Cartesian coordinate system with coordinates $\boldsymbol{x} = (x, y, z)$ for the streamwise, wall-normal and spanwise directions. The associated velocity components are given by $\boldsymbol{u} = (u, v, w)$. Within the framework of linear stability theory, the flow field variables $\boldsymbol{u}, p$ are assumed to be composed of laminar flow field variables $\boldsymbol{U} = (U, V, W), P$ superimposed with infinitesimal perturbation field variables $\boldsymbol{u}' = (u', v', w'), p'$, i.e.

$$\boldsymbol{u} = \boldsymbol{U} + \epsilon \boldsymbol{u}', \quad \text{with} \quad \epsilon \ll 1, \tag{2a}$$

$$p = P + \epsilon p'. \tag{2b}$$

Further, we analyze a parallel shear flow of the form

$$\boldsymbol{U} = (U(y), 0, 0), \tag{3}$$

Using Eq. (1a) and eliminating the pressure perturbation p', the Eqs. (1b) are linearized into two equations for the perturbation variables v', η', i.e.

$$\left[\left(\frac{\partial}{\partial t} + U \frac{\partial}{\partial x} \right) \nabla^2 - U'' \frac{\partial}{\partial x} - \frac{1}{Re} \nabla^4 \right] v' = 0, \tag{4a}$$

$$\left[\frac{\partial}{\partial t} + U \frac{\partial}{\partial x} - \frac{1}{Re} \nabla^2 \right] \eta' = -U' \frac{\partial v'}{\partial z}, \tag{4b}$$

where v' represents the wall-normal velocity perturbation, and η' denotes the wall-normal vorticity perturbation, defined by

$$\eta' = \frac{\partial u'}{\partial z} - \frac{\partial w'}{\partial x}. \tag{5}$$

The perturbation fields v', η' are expressed through the normal mode approach consisting of amplitude functions $\tilde{v}, \tilde{\eta}$ that depend solely on the inhomogeneous y-direction, together with an exponential function with the wave frequency ω in time t and wave numbers α and β in the homogeneous x- and z-directions, respectively

$$v'(x, y, z, t) = \tilde{v}(y) e^{i(\alpha x + \beta z - \omega t)}, \tag{6a}$$

$$\eta'(x, y, z, t) = \tilde{\eta}(y) e^{i(\alpha x + \beta z - \omega t)}. \tag{6b}$$

This ansatz corresponds to selecting a single Fourier-Laplace mode from the complete Fourier-Laplace representation of the initial-boundary value problem, which consists of a superposition of infinitely many such modes.

Substituting the normal-mode representation (6) into the governing equations (4) converts the spatiotemporal PDE system into the spectral ODE system

$$\left[(-i\omega + i\alpha U) \left(\frac{\mathrm{d}^2}{\mathrm{d}y^2} - \left(\alpha^2 + \beta^2\right) \right) - i\alpha U'' - \frac{1}{Re} \left(\frac{\mathrm{d}^2}{\mathrm{d}y^2} - \left(\alpha^2 + \beta^2\right) \right)^2 \right] \tilde{v} = 0, \tag{7a}$$

$$\left[(-i\omega + i\alpha U) - \frac{1}{Re} \left(\frac{\mathrm{d}^2}{\mathrm{d}y^2} - \left(\alpha^2 + \beta^2\right) \right) \right] \tilde{\eta} = -i\beta U' \tilde{v}, \tag{7b}$$

the first of which is the Orr-Sommerfeld equation (OSE), named after Orr (1907) and Sommerfeld (1909), while the second is the Squire equation (SE). In general, the spectral parameters $\omega, \alpha, \beta \in \mathbb{C}$ are complex, although other number sets like the real numbers $\mathbb{R}$ will also be considered.

BRIGGS' METHOD

The starting point of Briggs' method is the inverse Fourier-Laplace transform

$$v'(x, y, t) = \frac{1}{4\pi^2} \int_{\mathcal{L}_\omega} \int_{\mathcal{F}_\alpha} \tilde{v}(\alpha, y, \omega) e^{i(\alpha x - \omega t)} \, \mathrm{d}\alpha \, \mathrm{d}\omega. \tag{8}$$

The central concept of Briggs' method is that the asymptotic behavior of this inverse Fourier-Laplace transform (8) is governed by distinguished points in the complex wave number and wave frequency planes. These points are determined by examining how the eigenvalue spectra associated with the Green's function, proportional to $\tilde{v}$, change as the integration contours $\mathcal{L}_\omega$ and $\mathcal{F}_\alpha$ of the inverse Fourier-Laplace transform (8) are continuously deformed through the complex planes. Each point on an integration contour generates an entire eigenvalue spectrum in the other complex plane. For example, a wave number α on the spatial integration contour $\mathcal{F}_\alpha$ gives rise to a temporal eigenvalue spectrum. Among these, the dominant eigenvalue is the one with the largest imaginary part, corresponding to the highest temporal growth. Evaluating this dominant eigenvalue for all α in $\mathcal{F}_\alpha$, one obtains a temporal eigenvalue trajectory $\omega(\mathcal{F}_\alpha)$. An analogous construction applies to the temporal integration contour. Each wave frequency ω on $\mathcal{L}_\omega$ produces a spatial eigenvalue spectrum. In this instance, two spatial eigenvalues are followed from each spectrum, namely those eigenvalues located closest above and beloe spatial integration contour $\mathcal{F}_\alpha$. These two branches determine the topology of the integration contour. Evaluating these two branches for all ω in $\mathcal{L}_\omega$ generates two spatial eigenvalue trajectories, $\alpha_u(\mathcal{L}_\omega)$ above and $\alpha_l(\mathcal{L}_\omega)$ below the integration contour $\mathcal{F}_\alpha$.

Using the tools of complex analysis, the integration contours $\mathcal{L}_\omega$ and $\mathcal{F}_\alpha$ may be deformed continuously without altering the value of the inverse Fourier-Laplace transform (8), provided that the topology of the eigenvalue trajectories in the complex planes stays unchanged. This means in particular that eigenvalues initially situated above or below the integration contours must remain above or below respectively. At a pinch point α_p, where two spatial eigenvalue trajectories $\alpha_u(\mathcal{L}_\omega)$ and $\alpha_l(\mathcal{L}_\omega)$ coalesce, the spatial integration contour $\mathcal{F}_\omega$ is trapped between the two eigenvalue trajectories and can no longer be deformed without breaking the topology.

Since two eigenvalue branches coincide at a pinch point, the pinch point corresponds to a double root of the dispersion relation. At a double root, both the function itself and its first derivative vanish, which yields the conditions

$$\mathcal{D}(\alpha, \omega)\big|_{(\alpha_p, \omega_p)} = 0, \tag{9a}$$

$$\left.\frac{\partial \mathcal{D}(\alpha, \omega)}{\partial \alpha}\right|_{(\alpha_p, \omega_p)} = 0. \tag{9b}$$

Considering the inverse Fourier–Laplace transform in the form $\omega(\alpha)$, the phase of the exponential kernel becomes stationary with respect to α along a ray of constant observer velocity x/t. This condition reads

$$\frac{\partial(\alpha x-\omega t)}{\partial\alpha}=x-\frac{\mathrm{d}\omega}{\mathrm{d}\alpha}t\overset{!}{=}0, \tag{10a}$$

$$\Rightarrow\frac{\mathrm{d}\omega}{\mathrm{d}\alpha}=\frac{x}{t}. \tag{10b}$$

Applying implicit differentiation to the dispersion relation gives

$$\left.\frac{\mathrm{d}\omega}{\mathrm{d}\alpha}\right|_{(\alpha_p,\omega_p)}=-\left.\frac{\frac{\partial\mathcal{D}(\alpha,\omega)}{\partial\alpha}}{\frac{\partial\mathcal{D}(\alpha,\omega)}{\partial\omega}}\right|_{(\alpha_p,\omega_p)}=0, \tag{11}$$

where the final equality follows directly from the double-root condition (9b). Consequently, the associated group velocity vanishes at the pinch point. The point (α_p,ω_p) therefore represents a saddle point in the stationary reference frame corresponding to the ray $x/t=0$. Since the spatial integration contour passes through this saddle point along a direction of steepest descent, the spatial inverse transform can be evaluated asymptotically by means of the method of steepest descent.

The location of the corresponding ω_p in the complex frequency plane determines the type of instability. If $\omega_{p,i}>0$, perturbations grow in time at every fixed spatial location, corresponding to an absolute instability. In contrast, if $\omega_{p,i}<0$, disturbances decay in the stationary frame and the flow is stable with respect to that saddle point contribution. The temporal inverse transform may then be evaluated by closing the contour $\mathcal{L}_\omega$ and applying the residue theorem at ω_p.

The above formulation of Briggs' method is expressed in the stationary reference frame associated with the ray $x/t=0$. As a consequence, instabilities that are absolute only in a moving frame, corresponding to convective instabilities in the stationary frame, are not captured directly within this pinch point methodology. For these, the saddle points for different observer velocity, i.e. rays $x/t=\mathrm{const.}$ have to be found, which are in general not identical to a pinch point. Only for $x/t=0$, pinch point and saddle point come together.

NUMERICAL ALGORITHM

Evolution equations of the integration contours

The central idea of the proposed numerical method is to formulate evolution equations for the integration contours, thereby obtaining a geometric gradient-flow problem in the complex planes. Within this framework, the integration contours are interpreted as elastic curves that experience a repulsive interaction from the eigenvalue trajectories generated by the respective complementary integration contour.

The integration contours are continuously deformed over a pseudo-time τ, which serves as an optimization parameter relaxing the contours toward an optimal configuration.

To this end, the integration contours are represented as functions in the complex plane, by assigning an imaginary part to each value of the real coordinate. For the temporal integration contour $\mathcal{L}_\omega$, the imaginary part is constant for all real wave frequencies, such that the contour forms and remains a horizontal straight line throughout the evolution. In contrast, the spatial integration contour $\mathcal{F}_\alpha$ allows the imaginary part to vary along the contour,

$$\mathcal{L}_\omega:\mathbb{R}\to\mathbb{C},\quad \omega_r\mapsto\omega=\omega_r+i\omega_i, \tag{12a}$$

$$\mathcal{F}_\alpha:\mathbb{R}\to\mathbb{C},\quad \alpha_r\mapsto\alpha=\alpha_r+i\alpha_i(\alpha_r). \tag{12b}$$

We propose that the contour dynamics are governed by the following set of evolution equations

$$\partial_\tau\mathcal{L}_\omega=-\boldsymbol{n}\left(\nabla_{\boldsymbol{n}}\Phi_{\mathcal{L}_\omega}+\sigma_{\mathrm{curv}}\kappa\right)-i\lambda+\boldsymbol{t}\cdot\boldsymbol{v}_\parallel, \tag{13a}$$

$$\partial_\tau\mathcal{F}_\alpha=-\boldsymbol{n}\left(\nabla_{\boldsymbol{n}}\Phi_{\mathcal{F}_\alpha}+\sigma_{\mathrm{curv}}\kappa\right)+\boldsymbol{t}\cdot\boldsymbol{v}_\parallel. \tag{13b}$$

The potential function Φ in Eq. (13) measures the proximity between a point on an integration contour and the eigenvalue trajectory or trajectories associated with the opposite integration contour. Through the directional derivative $-\nabla_{\boldsymbol{n}}$, the contours are driven away from these trajectories so as to maximize their separation. Since only motion in the normal direction modifies the shape of a contour, whereas tangential motion merely changes its parametrization, all physically relevant forces are projected onto the unit normal vector $\boldsymbol{n}$.

The next term in Eq. (13) contains the contour curvature κ together with a curvature-penalty coefficient σ_{curv}. This term acts as a regularization mechanism, suppressing large curvatures and preventing the formation of cusps or strong high-frequency oscillations, thereby promoting smooth contour geometries.

For the temporal integration contour, the term $-i\lambda$ in Eqs. (13) introduces a uniform downward translation in the complex ω-plane. It acts as a Lagrange multiplier controlling the imaginary level of the contour and directly implements the fundamental principle of Briggs' method, namely lowering the temporal contour as far as admissibly possible.

The tangential velocity $\boldsymbol{v}_\parallel$, projected onto the unit tangent vector $\boldsymbol{t}$, serves only as a reparametrization control and disappears from the final form of the evolution equations.

The geometric quantities appearing in the evolution equations (13) can be expressed in terms of the contour functions $f\in\omega_i,\alpha_i(\alpha_r)$ as

$$\boldsymbol{n}=\frac{-f'+i}{\sqrt{1+(f')^2}}, \tag{14a}$$

$$\boldsymbol{t}=\frac{1+if'}{\sqrt{1+(f')^2}}, \tag{14b}$$

$$\kappa=\boldsymbol{\nabla}\cdot\boldsymbol{n}=\frac{-f''}{\left(1+(f')^2\right)^{\frac{3}{2}}}, \tag{14c}$$

$$\nabla_{\boldsymbol{n}}=\boldsymbol{n}\cdot\boldsymbol{\nabla}. \tag{14d}$$

With that, the evolution equations (13) can be rewritten as

$$\partial_\tau\omega_i=-\frac{\partial\Phi_{\mathcal{L}_\omega}}{\partial\omega_i}-\lambda, \tag{15a}$$

$$\partial_\tau\alpha_i=\left(\frac{\mathrm{d}\alpha_i}{\mathrm{d}\alpha_r}\frac{\partial\Phi_{\mathcal{F}_\alpha}}{\partial\alpha_r}-\frac{\partial\Phi_{\mathcal{F}_\alpha}}{\partial\alpha_i}\right)+\frac{\sigma_{\mathrm{curv}}\frac{\mathrm{d}^2\alpha_i}{\mathrm{d}\alpha_r^2}}{1+\left(\frac{\mathrm{d}\alpha_i}{\mathrm{d}\alpha_r}\right)^2}. \tag{15b}$$

Note that the derivative terms of $\mathrm{d}\omega_i/\mathrm{d}\omega_r$ and $\mathrm{d}^2\omega_i/\mathrm{d}\omega_r^2$ have vanished, since the temporal integration contour is a horizontal straight line. The global potential functions are chosen as

$$\Phi_{\mathcal{L}_\omega}(\omega)=\int_{\omega(\mathcal{F}_\alpha)}\varphi\left(\left|\omega-\omega'\right|\right)\left|\mathrm{d}\omega'\right|, \tag{16a}$$

$$\Phi_{\mathcal{F}_\alpha}(\alpha)=\sum_{j\in\{u,l\}}\int_{\alpha_j(\mathcal{L}_\omega)}\varphi\left(\left|\alpha-\alpha'\right|\right)\left|\mathrm{d}\alpha'\right|. \tag{16b}$$

For every point on an integration contour, these potentials quantify its interaction with the corresponding eigenvalue trajectories. This is achieved by integrating a local interaction potential φ along the complete eigenvalue trajectory.

The local potential functions are chosen as a smooth analytic expression with exponentially decaying influence at large distances,

$$\varphi(r) = e^{\frac{\zeta}{r^2+\varepsilon}} - 1. \tag{17}$$

The parameter $\zeta \in \mathbb{R}^+$ determines the effective range of the interaction. Larger values of ζ produce a stronger and more localized repulsion, whereas smaller values yield a broader interaction region with reduced intensity. The parameter ε serves as a regularization term that removes the singularity at $r = 0$. Consequently, φ and all of its derivatives remain analytic even when the integration contour locally coincides with an eigenvalue trajectory. The derivative of the local potential is given analytically by

$$\frac{\mathrm{d}\varphi(r)}{\mathrm{d}r} = -\frac{2\zeta r}{(r^2+\varepsilon)^2}\, e^{\frac{\zeta}{r^2+\varepsilon}}\,, \tag{18}$$

which leads to the following expressions for the derivatives of the global potentials,

$$\frac{\partial \Phi_{\mathcal{L}_\omega}(\omega)}{\partial \omega_i} = \int_{\omega(\mathcal{F}_\alpha)} \frac{\omega_i - \omega_i'}{|\omega-\omega'|^2}\frac{\mathrm{d}\varphi\left(|\omega-\omega'|\right)}{\mathrm{d}\,|\omega-\omega'|}\left|\mathrm{d}\omega'\right|, \tag{19a}$$

$$\frac{\partial \Phi_{\mathcal{F}_\alpha}(\alpha)}{\partial \alpha_r} = \sum_{j\in\{u,l\}}\int_{\alpha_j(\mathcal{L}_\omega)} \frac{\alpha_r - \alpha_r'}{|\alpha-\alpha'|^2}\frac{\mathrm{d}\varphi\left(|\alpha-\alpha'|\right)}{\mathrm{d}\,|\alpha-\alpha'|}\left|\mathrm{d}\alpha'\right|, \tag{19b}$$

$$\frac{\partial \Phi_{\mathcal{F}_\alpha}(\alpha)}{\partial \alpha_i} = \sum_{j\in\{u,l\}}\int_{\alpha_j(\mathcal{L}_\omega)} \frac{\alpha_i - \alpha_i'}{|\alpha-\alpha'|^2}\frac{\mathrm{d}\varphi\left(|\alpha-\alpha'|\right)}{\mathrm{d}\,|\alpha-\alpha'|}\left|\mathrm{d}\alpha'\right|. \tag{19c}$$

Discrete symmetries

To reduce the portion of the complex planes that must be explored numerically, the discrete symmetries of the sytem of spectral governing equations (7), written in the form $\mathcal{L}\tilde{v} = 0$, are exploited. These symmetries should not be confused with the continuous symmetries employed in Lie-group analysis.

The first discrete symmetry is complex conjugation. Complex conjugation $\overline{(\cdot)}$ yields $\overline{\mathcal{L}}\overline{\tilde{v}} = 0$. The complex conjugate of the differential operator $\overline{\mathcal{L}}$ only affects the complex spectral parameters (α, ω) to $(\overline{\alpha}, \overline{\omega})$. Like so, it follows that the eigenvalues of $\mathcal{L}$ and $\overline{\mathcal{L}}$ are related as

$$\mathcal{D}(\alpha,\omega) = \mathcal{D}(\overline{\alpha},\overline{\omega}) = 0. \tag{20}$$

The second discrete symmetry is the reversal of the normal mode phase in space and time, which follows from the normal mode approach (6). A complex conjugate normal mode corresponds to the physical field

$$e^{\overline{i}(\overline{\alpha}x - \overline{\omega}t)} = e^{i[(-\overline{\alpha})x-(-\overline{\omega})t]}, \tag{21}$$

which is itself again a normal mode with spectral parameters $(-\overline{\alpha}, -\overline{\omega})$. Therefore, the dispersion relation is also symmetric with respect to

$$\mathcal{D}(\alpha,\omega) = \mathcal{D}(-\overline{\alpha},-\overline{\omega}) = 0. \tag{22}$$

Combining those two discrete symmetries yields

$$\mathcal{D}(\alpha,\omega) = \mathcal{D}(-\alpha,-\omega) = \mathcal{D}(\overline{\alpha},\overline{\omega}) = \mathcal{D}(-\overline{\alpha},-\overline{\omega}) = 0. \tag{23}$$

Consequently, it is sufficient to restrict the investigation to a representative complex half-plane for one spectral parameter. We choose the right half-α-plane $\alpha_r \geq 0$, with the full ω-plane. The remaining region in the complex planes can then be recovered by applying the symmetry relations (23).

Numerical implementation

The integration contours are discretized by sampling the real axis at a finite number of points N_ω, N_α. A uniform discretization is introduced in the intervals $[\omega_{r,\min}, \omega_{r,\max}]$ and $[0, \alpha_{r,\max}]$, where $(\cdot)_{(j)}$ denotes a discretized point on an integration contour in the complex plane. The spatial derivatives are approximated with central finite difference quotients as

$$\frac{\mathrm{d}\alpha_{i,(j)}}{\mathrm{d}\alpha_r} = \frac{\alpha_{i,(j+1)} - \alpha_{i,(j-1)}}{\alpha_{r,(j+1)} - \alpha_{r,(j-1)}}, \tag{24a}$$

$$\frac{\mathrm{d}^2\alpha_{i,(j)}}{\mathrm{d}\alpha_r^2} = \frac{\alpha_{i,(j+1)} - 2\alpha_{i,(j)} + \alpha_{i,(j-1)}}{\left(\alpha_{r,(j+1)} - \alpha_{r,(j)}\right)\left(\alpha_{r,(j)} - \alpha_{r,(j-1)}\right)}, \tag{24b}$$

where the endpoints respectively use forward or backward finite difference quotients. The pseudo-time derivative is approximated with a forward finite difference quotient, i.e. explicit, with pseudo-time step length Δ_τ, where $(\cdot)^{(n)}$ denotes a discretized point in pseudo-time, as

$$\partial_\tau \omega_{i,(j)}^{(n)} = \frac{\omega_{i,(j)}^{(n+1)} - \omega_{i,(j)}^{(n)}}{\Delta\tau}, \tag{25a}$$

$$\partial_\tau \alpha_{i,(j)}^{(n)} = \frac{\alpha_{i,(j)}^{(n+1)} - \alpha_{i,(j)}^{(n)}}{\Delta\tau}. \tag{25b}$$

The pseudo-time evolution is continued until convergence, defined by

$$\max_j \left|\alpha_{i,(j)}^{(n+1)} - \alpha_{i,(j)}^{(n)}\right| < \delta, \tag{26}$$

with a prescribed tolerance δ. At convergence, the integration contours are stationary solutions of the geometric evolution equations and represent admissible Briggs integration contours for the subsequent asymptotic analysis.

Pseudo-time step

We propose adaptive time stepping via a variable pseudo-time step size $\Delta\tau$. For the spatial contour, the local pseudo-time step is decreased when the upper and lower spatial branches approach each other. The branch distance d_{branch} is computed via

$$d_{\mathrm{branch}} = \min_j \left|\alpha_{u,j} - \alpha_{l,j}\right|. \tag{27}$$

The local pseudo-time step is chosen as

$$\Delta\tau_{\mathrm{loc}} = \Delta\tau \max\left\{0.1, \min\left\{\frac{d_{\mathrm{branch}}}{d_{\mathrm{safe}}}, 1\right\}\right\}, \quad d_{\mathrm{safe}} = 0.2. \tag{28}$$

In this way, the contour evolution slows as the two spatial branches approach each other towards a possible pinch point.

Safety mechanisms

In addition to the adaptive pseudo-time step, several numerical safeguards are used during the contour evolution. The upper and lower spatial branches are classified using the local normal direction of the spatial contour. For a spatial eigenvalue α, the nearest contour point $\mathcal{F}_{\alpha,j}$ and its unit normal n_j are used to compute the projection

$$\mathrm{proj}_j = \mathrm{Re}\left[\overline{n_j}\,(\alpha - \mathcal{F}_{\alpha,j})\right]. \quad (29)$$

Eigenvalues with $\mathrm{proj}_j > 0$ are assigned to the upper branch, while those with $\mathrm{proj}_j < 0$ are assigned to the lower branch. The temporal contour is also constrained to remain above the temporal eigenvalue trajectory. Therefore, its imaginary level must satisfy

$$\omega_i > \max_j \mathrm{Im}\left(\omega(\mathcal{F}_\alpha)\right) + \varepsilon. \quad (30)$$

If a trial update violates this condition, or if the contour motion becomes too large, the update is rejected, and the pseudo-time step is reduced, for example by

$$\Delta\tau \leftarrow \frac{1}{2}\Delta\tau. \quad (31)$$

Finally, after each accepted spatial update, a mild smoothing is applied to the spatial contour with a rolling average filter.

Analytic test case for algorithm validation

The algorithm is applied to the analytic test equation similar to Sengupta & Orkwis (1996). We choose a simple analytic test equation linear in ω and quadratic in α, i.e. of the type

$$\mathcal{D}(\alpha,\omega) = \omega - C_0 - C_1\alpha - C_2\alpha^2 = 0, \quad (32)$$

with the analytic roots $\omega = C_0 + C_1\alpha + C_2\alpha^2$ and $\alpha = (-C_1 \pm \sqrt{C_1^2 - 4C_2(C_0-\omega)})/(2C_2)$. The analytic pinch point then lies at

$$(\alpha_p,\omega_p) = \left(-\frac{C_1}{2C_2}, C_0 - \frac{C_1^2}{4C_2}\right). \quad (33)$$

Table 1: Parameters used for the analytic test function.

Parameter	Value	Parameter	Value
C_0	$-1.0+0.96i$	λ	4.0
C_1	$0.4+0.8i$	$\Delta\tau$	10^{-3}
C_2	1.0	σ_{curv}	3×10^{-5}
ζ	4×10^{-4}	ε	10^{-10}
N	141	d_{safe}	0.05

The parameters used in the test case are summarized in Table 1.

For the analytical test equation, Figure 1 shows the corresponding contour evolution. Starting from the initial integration contours, the temporal contour is lowered while the spatial contour is deformed. During this process, the upper and lower spatial branches approach each other and finally meet near the analytically known pinch point.

CONCLUSIONS & OUTLOOK

A novel numerical framework for the application of Briggs' method to linear stability theory has been presented. Instead of searching directly for double roots of the dispersion relation, the method formulates the contour-deformation process itself as a geometric evolution problem in the complex wave number and wave frequency planes. The spatial and temporal integration contours of the inverse Fourier-Laplace contours are treated as evolving curves that interact with the associated eigenvalue trajectories through repulsive potential functions.

The resulting evolution equations preserve the topological constraints underlying Briggs' method while continuously deforming the contours toward optimal admissible configurations,i.e. pinch points in Briggs' method.

The proposed algorithm has been verified using an analytic test dispersion relation possessing a known analytic pinch point. The numerical contour evolution successfully converged toward the analytically predicted double-root location, demonstrating the feasibility of the approach and validating the underlying geometric formulation.

Future work will focus on applying the method to the Orr-Sommerfeld equation for plane Couette flow. Particular emphasis will be placed on the identification of spatiotemporal pinch points associated with oblique disturbances and on assessing their implications within the framework of the recently developed extension of Squire's theorem to spatiotemporal normal modes. Beyond plane Couette flow, the geometric contour-evolution framework may provide a general tool for the analysis of spatiotemporal instability problems in more complex shear flows.

REFERENCES

Bers, A. 1983 Space-time evolution of plasma instabilities - absolute and convective. In *Handbook of Plasma Physics, Vol. 1: Basic Plasma Physics I* (ed. M. N. Rosenbluth & R. Z. Sagdeev), pp. 451–517. Amsterdam: North-Holland.

Briggs, R. J. 1964 *Electron-stream interaction with plasmas*. The MIT Press.

Deissler, R. J. 1987 The convective nature of instability in plane Poiseuille flow. *Physics of Fluids* **30** (8), 2303–2305.

Oberlack, M., Wilhelm, K. V., Görtz, S., Conrad, J., Yalcin, A., De Broeck, L. & Wang, Y. 2026 New subcritical oblique modes: On an extension of squire's theorem for spatiotemporally evolving modes. *Physical Review Fluids* **11**, 043902.

Orr, W. M. 1907 The stability or instability of the steady motions of a perfect liquid and of a viscous liquid. Part II: A viscous liquid. *Proceedings of the Royal Irish Academy. Section A: Mathematical and Physical Sciences* **27**, 69–138.

Sengupta, R. & Orkwis, P. D. 1996 An efficient numerical technique for capturing saddle points of dispersion relations. In *Theoretical Fluid Mechanics Conference*. American Institute of Aeronautics and Astronautics, 1st AIAA Theoretical Fluid Mechanics Meeting, June 17–20, 1996 New Orleans, LA. AIAA Meetings Paper on Disc, June 1996. A9636575, AIAA Paper 96-2158.

Sommerfeld, A. 1909 Ein Beitrag zur hydrodynamischen Erklärung der turbulenten Flüssigkeitsbewegungen. In *Atti del IV Congresso Internazionale dei Matematici*. Rome: Tipografia della R. Accademia dei Lincei.

Squire, H. B. 1933 On the stability for three-dimensional disturbances of viscous fluid flow between parallel walls. *Proceedings of the Royal Society of London. Series A, Containing Papers of a Mathematical and Physical Character* **142** (847), 621–628.

Wilhelm, K. V., Conrad, J., Oberlack, M. & Wang, Y. 2026 Symmetries in linear stability theory and their implications for the dispersion relation. *under review at Physical Review E* pp. –.

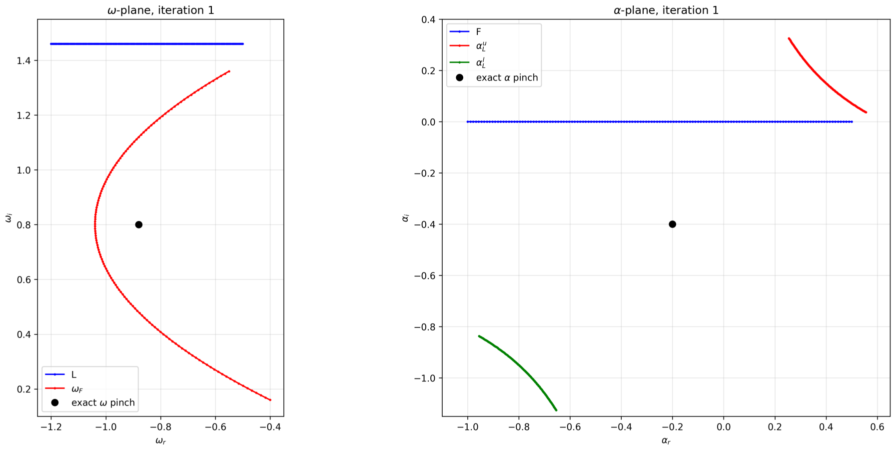

(a) Initial contours for the analytic test function

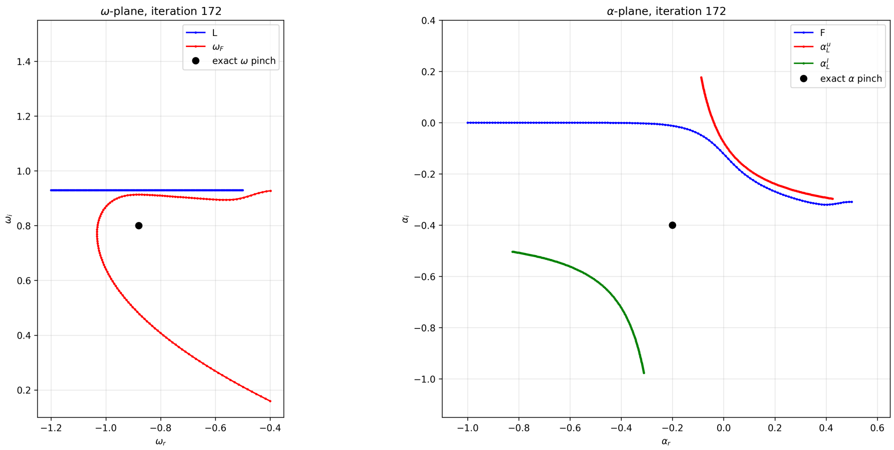

(b) Intermediate deformation of the test-function contours

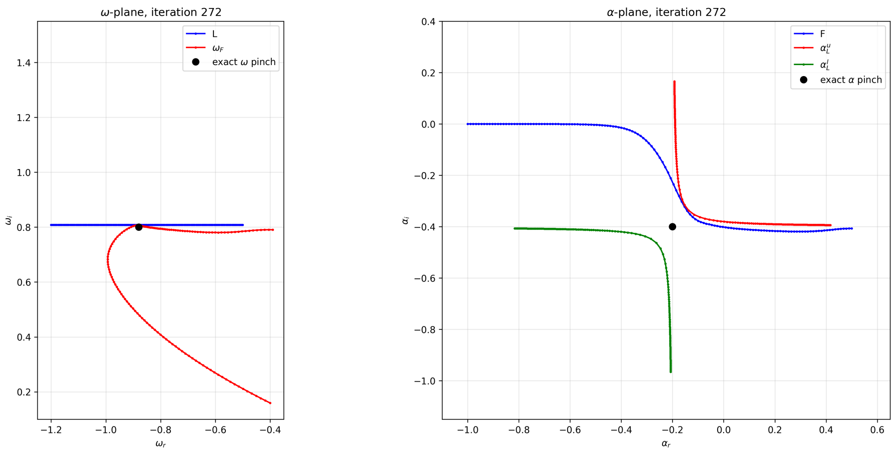

(c) Approach of the test-function branches toward the pinch point

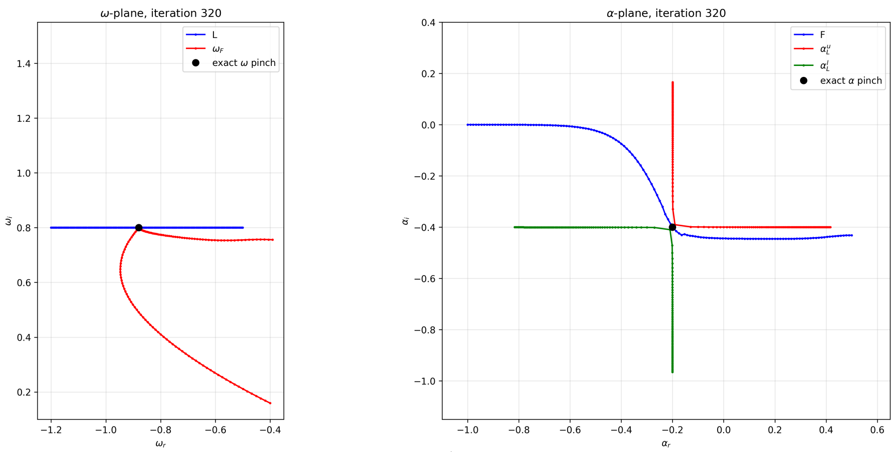

(d) Final test-function configuration near the analytic pinch point

Figure 1: Contour evolution for the analytic test function